Langmuir

ARTICLE

pubs.acs.org/Langmuir

Adsorption-Induced Deformation of Mesoporous Solids: Macroscopic Approach and Density Functional Theory

Gennady Yu. Gor and Alexander V. Neimark*

Department of Chemical and Biochemical Engineering, Rutgers, The State University of New Jersey, 98 Brett Road, Piscataway, New Jersey 08854-8058, United States

ABSTRACT: We present a theoretical study of the deformation of mesoporous solids during adsorption. The proposed thermodynamic model allows one to link the mechanical stress and strain to the solvation pressure exerted by the adsorbed molecules on the pore wall. Two approaches are employed for calculation of solvation pressure as a function of adsorbate pressure: the macroscopic Derjaguin–Broekhoff–de Boer theory of capillary condensation, and the microscopic density functional theory. We revealed that the macroscopic and microscopic theories are in quantitative agreement for the pores >8 nm diameter within the whole range of adsorbate pressures. For smaller pores, the macroscopic theory gradually deteriorates, and the density functional theory extends the thermodynamic model of adsorption-induced deformation to the nanometer scales.

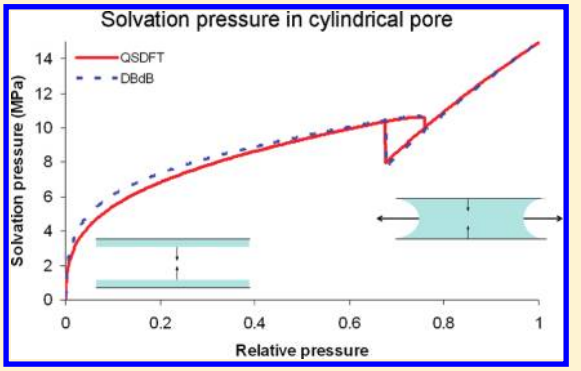

1. INTRODUCTION

In the course of gas adsorption or desorption, the volume of adsorbents changes. This phenomenon is known in the literature as adsorption-induced deformation. It is hard to refer to the first observations of adsorption-induced deformation, but as early as in the 18th century this effect was already implemented in an instrument. De Saussure employed the property of a human hair to expand with the increase of air humidity in his hair hygrometer.[1] This effect was explained by the action of capillary forces using the Kelvin–Laplace equation that related the capillary pressure to humidity[2] (see ref 3 for review).

Adsorption-induced deformation is a ubiquitous phenomenon observed in various systems: charcoal,[4,5] activated carbon,[6] porous glass,[7−9] zeolites,[10−12] silica gels,[13] and porous silicon.[14] Recently, the interest in scientific studies of the specifics of adsorption-induced deformation has revived due to the opportunities offered by novel nanoporous materials, such as mesoporous crystals and metal–organic frameworks (MOFs), which possess crystallographically ordered morphologies, and modern experimental techniques, such as ellipsometric porosimetry[15] and in situ small-angle X-ray and neutron diffractometry,[16] which allow one to obtain high-resolution data for theoretical analyses. While a rich collection of experimental data is currently available, the theoretical understanding of adsorption-induced deformation is still far from being completed. In particular, the most recent findings of breathing transitions in MOFs[17] facilitated development of novel thermodynamic approaches to coupling adsorption and deformation processes.[18]

The classical experiments on adsorption on charcoal demonstrated monotonic swelling of samples upon adsorption[19] that was explained in terms of the so-called Bangham effect:[20] adsorption causes a gradual decrease of the surface free energy or surface tension of the pore walls. However, the deformation behavior of mesoporous solids, which is the main subject of the current paper, is more complicated. In particular, Amberg and McIntosh[7] showed that, in general, deformation is not necessarily monotonic and may exhibit alternating stages of expansion and contraction in the course of adsorption. Moreover, deformation in the process of desorption reveals a prominent hysteresis coupled with the adsorption–desorption hysteresis. The authors[7] explained the nonmonotonic deformation of porous glass by a competition of capillary and Bangham effects. Such characteristic nonmonotonic deformation was later observed for many other systems.[14,21−25]

In a recent letter,[26] we presented a thermodynamic approach to adsorption-induced deformation of mesoporous solids, based on the Derjaguin–Broekhoff–de Boer (DBdB) theory of capillary condensation.[27−29] The DBdB theory allowed us to obtain an analytical description of the adsorption stress and respective strain for a model adsorbent with cylindrical pores. While the results of the DBdB theory are in line with the qualitative description of Amberg and McIntosh[7] and give good agreement with recent experimental data,[24] they have a serious limitation due to the macroscopic nature of basic equations.[30] Adsorption isotherms calculated with the DBdB theory are in quantitative agreement with experimental data and results of microscopic approaches based on Monte Carlo (MC) simulations or the density functional theory (DFT) only for pores larger than ∼7–8 nm.[31] For smaller pores, the DBdB predictions gradually deteriorate.

Received: April 6, 2011
Revised: May 3, 2011
Published: May 13, 2011

ACS Publications © 2011 American Chemical Society

In the current study in order to extend this approach to smaller pore sizes, we employ the quenched solid density functional theory (QSDFT).[32,33] Our goal is to obtain deformation curves based on QSDFT, and, as such, to build a bridge between the intuitively transparent macroscopic theory[26] and the microscopic description. The structure of the paper is as follows: In Section 2, the thermodynamic approach to adsorption-induced deformation is formulated. A brief overview of the DBdB theory and its application is given in Section 3. Section 4 presents the formulation of the QSDFT model. Section 5 contains the results of calculations and a discussion of the QSDFT and DBdB predictions of adsorption and stain isotherms.

2. THERMODYNAMIC MODEL OF ADSORPTION-INDUCED DEFORMATION

While describing the adsorption-induced deformation of porous solids, two different scales should be addressed. The stress exerted on the pore walls by the adsobed molecules (adsorption stress) is calculated on the single pore level. The elastic response of the porous body is calculated either using the macroscopic elasticity theory[34] or applying Biot's theory of poroelasticity.[35,36] As we revealed in our preceding study,[26] for mesoporous solids, which are relatively rigid and have narrow pore size distribution (such as glasses or silica mesoporous crystals), a detailed examination of the elastic response is not necessary. Deformation of these systems can be described within a framework of the thermodynamic model, which was employed earlier for description of deformation of zeolites,[37] microporous carbons,[38] MOFs[18] and coal.[39] This model assumes that Hooke's law is fulfilled for the sample as a whole, and that the solvation pressure f_s determines the magnitude of elastic deformation:

$$\varepsilon = \frac{1}{K}(f_s - \sigma_0) \tag{1}$$

Here ε is the volumetric strain ($\varepsilon = \Delta V/V$, where ΔV is the variation of the pore volume), K is the effective elastic modulus, and σ_0 is the pre-stress in the reference state, at which the initial pore volume V is defined. Solvation pressure is determined as the difference between the adsorption stress σ_s and the external pressure P, $f_s = \sigma_s - P$.[40] Adsorption stress is quantified as the derivative of the grand thermodynamic potential Ω of the adsorbed phase with respect to the pore volume V at fixed temperature T and adsorbate chemical potential μ:

$$\sigma_s = -\left(\frac{\partial \Omega}{\partial V}\right)_{\mu,T} \tag{2}$$

Therefore, to predict the sample strain, it is sufficient to know the solvation pressure f_s, or the adsorption stress σ_s. Using eq 2, the latter can be obtained from the grand potential Ω. Thus, the main theoretical problem is the determination of the grand thermodynamic potential $\Omega(\mu,V,T)$ of the adsorbate as a function of the external thermodynamic variables T and μ and the pore volume V. This can be done using a certain model of the adsorption process.

Before discussing the general situation, we should note that for a particular case of large mesopores at high adsorbate pressures, a simple capillary approximation can be used for the description of adsorption-induced deformation. Here, and below in this paper, we will assume the cylindrical geometry for the pores: R is the pore radius, L is the length of the pore, which is assumed to be sufficiently long, $L \gg R$. After the adsorbate pressure P exceeds the capillary condensation pressure P_c, but is still lower than the saturation pressure P_0 (i.e., $P_c < P < P_0$), the pore is filled with the condensed adsorbate except for concave menisci at the pore entrances (Figure 1). In this case (referred to as "filled pore" below) the Laplace pressure γ/R_m (γ is the liquid−vapor surface tension, R_m is the radius of meniscus) is acting outward, contracting the pore and the sample as a whole. The solvation pressure in this case is equal to the Laplace pressure that is obtained from the Kelvin−Laplace equation

Figure 1. Adsorption stress of the filled pore.

$$f_s = (R_g T/V_L)\ln(P/P_0) \tag{3}$$

where R_g is the gas constant, and V_L is the molar volume of the condensed phase.

The Laplace pressure decreases with the increase of adsorbate pressure, therefore the sample expands with the growth of P. It is worth noting that the capillary pressure (eq 3) does not depend on the specifics of the porous solid and, as such, is universal. It is this simple principle, which not only stays behind the hair hygrometer,[3] but also is widely used for processing results of adsorption-deformation experiments,[22,23,41] particularly for deriving the values of elastic modulus K of mesoporous samples. However, the capillary approximation cannot predict the adsorption stress for adsorbate pressures prior to capillary condensation in the so-called film region, when adsorbate forms an adsorbed film on the pore walls. The DBdB theory of capillary condensation helped us overcome this limitation.[26]

3. DBDB THEORY OF CAPILLARY CONDENSATION

Capillary approximation does not take into account solid−fluid interactions, and it cannot give any predictions for the solvation pressure in the film region of adsorption isotherm, where these interactions are dominant. The DBdB theory[27−29] is capable of predicting the whole adsorption isotherm quantitatively.[31] It employs Derjaguin's concept of disjoining pressure to describe the thermodynamic properties of adsorption film. Within the DBdB theory, the chemical potential μ of the film of thickness h adsorbed on the surface of a cylindrical pore is given by the following equation:

$$\mu = R_g T \ln(P/P_0) = -\left(\Pi(h) + \frac{\gamma}{R-h}\right)V_L \tag{4}$$

where $\Pi = \Pi(h)$ is the disjoining pressure. Two terms in the brackets on the right hand side of eq 4 represent two uncoupled contributions to the chemical potential: disjoining (related only to the film thickness h) and capillary (related only to the internal radius of film curvature $R - h$). Equation 4 assumes than the adsorbed phase is incompressible (V_L = const) and the gas phase is ideal.

Disjoining pressure isotherm $\Pi(h)$ can be obtained from adsorption experiments on a plain nonporous surface. For the cases of argon and nitrogen adsorption on silica, considered below, it is well approximated with the Frenkel−Halsey−Hill equation:[42−44]

dx.doi.org/10.1021/la201271p |Langmuir 2011, 27, 6926–6931

Table 1. Macroscopic Parameters of Nitrogen and Argon Adsorption on a Silica Surface[30]

adsorbate	γ (mN/m)	V_L (cm^3/mol)	k	m
N_2 at 77.4 K	8.88	34.66	44.54	2.241
Ar at 87.3 K	12.5	28.68	73.17	2.665

$$\Pi(h) = \frac{R_g T}{V_L}\frac{k}{(h/h_0)^m} \tag{5}$$

where $h_0 = 1$ Å, and k and m are empirical parameters. Values of k, m, and V_L for argon and nitrogen are given in Table 1.

As the adsorbate pressure P increases in the adsorption experiment, the film thickness h grows. The two contributions to the chemical potential (eq 4) compete: the disjoining pressure $\Pi(h)$ decreases, and the capillary pressure $\gamma/(R-h)$ increases. Therefore, at a certain value of pressure P_c, the film becomes unstable and the spontaneous capillary condensation takes place. The corresponding film thickness h_c can be obtained from the condition of the chemical potential maximum, as the solution of the following equation:

$$\left.\frac{d\Pi(h)}{dh}\right|_{h=h_c} + \frac{\gamma}{(R-h_c)^2} = 0 \tag{6}$$

At pressure values $P > P_c$, the pore is filled, and the deformation can be treated in the capillary approximation (eq 3).

In the desorption process, the pressure P decreases starting from the filled pore region, and the capillary evaporation takes place upon the formation of the equilibrium meniscus at $P = P_e$ ($P_e < P_c$). The value of P_e, along with the corresponding film thickness h_e, can be obtained from the Derjaguin equation:[29]

$$R_g T \ln(P_e/P_0) = -2V_L\left[\frac{\gamma}{R-h_e} + \frac{1}{(R-h_e)^2}\int_{h_e}^{R}(R-h')\Pi(h')\,dh'\right] \tag{7}$$

During desorption from the film at $P < P_e$, the chemical potential of the system μ is interrelated with the film thickness by means of eq 4. Therefore, deriving P_e and P_c from eqs 6 and 7, using eq 4, one can construct the whole adsorption isotherm (see Section 5).

Variation of the grand potential of the system along the isotherm is related to the adsorption isotherm through the Gibbs equation

$$\Omega(P) = \Omega(P_0) - \int_0^{\mu(P)} N(\mu')\,d\mu' \tag{8}$$

Thus, the DBdB theory allows one to obtain from eqs 2, 8, 4, and 5 the analytical expressions for the solvation pressure both in the film (f_s^f) and filled pore (f_s^c) regions of adsorption isotherms:[26]

$$f_s^c(P) = -\frac{\gamma_{sl}}{R} + \frac{R_g T}{V_L}\ln\left(\frac{P}{P_0}\right) + (P_0 - P) \tag{9}$$

$$f_s^f(h) = -\frac{\gamma_{sl}}{R} - P - \frac{\gamma}{R-h} - \frac{R_g T}{V_L}k\frac{m}{m-1}\frac{h_0}{R}\left(\frac{h}{h_0}\right)^{1-m} \tag{10}$$

where γ_{sl} is the solid−liquid surface tension.

4. QUENCHED SOLID DENSITY FUNCTIONAL THEORY

QSDFT, developed recently,[32,33] provides a coherent description of adsorption on amorphous surfaces. In contrast to the conventional nonlocal DFT,[45,46] QSDFT accounts for the molecular roughness of the solid surface. QSDFT considers a two-component system, where the solid is modeled as a compound of hardcore spheres, interacting with the fluid molecules via a pairwise attractive potential. The QSDFT grand thermodynamic potential of the solid−fluid system Ω_{sf} is written as[32,33]

$$\begin{aligned}\Omega_{sf}[\rho_s(\mathbf{r}),\rho_f(\mathbf{r})] = {} & F_{id}[\rho_f(\mathbf{r})] + F_{id}[\rho_s(\mathbf{r})] + F_{ex}[\rho_s(\mathbf{r}),\rho_f(\mathbf{r})] \\ & + \frac{1}{2}\int\int d\mathbf{r}d\mathbf{r}'\rho_f(\mathbf{r})\rho_f(\mathbf{r}')u_{ff}(|\mathbf{r}-\mathbf{r}'|) \\ & + \frac{1}{2}\int\int d\mathbf{r}d\mathbf{r}'\rho_s(\mathbf{r})\rho_s(\mathbf{r}')u_{ss}(|\mathbf{r}-\mathbf{r}'|) \\ & + \iint d\mathbf{r}d\mathbf{r}'\rho_f(\mathbf{r})\rho_s(\mathbf{r}')u_{sf}(|\mathbf{r}-\mathbf{r}'|) \\ & - \mu_f\int d\mathbf{r}\rho_f(\mathbf{r}) - \mu_s\int d\mathbf{r}\rho_s(\mathbf{r})\end{aligned} \tag{11}$$

Here $\mathbf{r}$ and $\mathbf{r}'$ are the position vectors, $\rho_f(\mathbf{r})$ and $\rho_s(\mathbf{r})$ are the fluid and solid density profiles, $F_{id}[\rho_f(\mathbf{r})]$ and $F_{id}[\rho_s(\mathbf{r})]$ are the ideal contributions of hard-sphere repulsive free energy for the fluid and solid components, $F_{ex}[\rho_s(\mathbf{r}),\rho_f(\mathbf{r})]$ is the excess free energy term for both solid and fluid components, $u_{ff}(r)$, $u_{ss}(r)$, $u_{sf}(r)$ are the attractive parts of the fluid−fluid, solid−solid, and solid−fluid potentials, respectively (r is the distance between two particles), and μ_f and μ_s are the chemical potentials of the fluid and solid.

The key term of the QSDFT approach in eq 11 is the excess free energy of the solid−fluid hard spheres mixture, $F_{ex}[\rho_s(\mathbf{r}),\rho_f(\mathbf{r})]$. We employ Rosenfeld's fundamental measure theory[47] in its version,[48] which is consistent with the Percus−Yevick equation of state for bulk hard spheres fluid (see details in ref 33). The QSDFT model assumes that the distribution of solid density does not change in the process of adsorption and, as such, is "quenched". The equilibrium fluid density distribution is found from the condition of minimization of the grand thermodynamic potential with respect to the fluid density, while the solid density and the external thermodynamic conditions of T and μ are kept fixed,

$$\left.\frac{\delta\Omega[\rho_s(\mathbf{r}),\rho_f(\mathbf{r})]}{\delta\rho_f(\mathbf{r})}\right|_{\rho_s(\mathbf{r})} = 0 \tag{12}$$

which leads to the solution of the Euler−Lagrange equation

$$\begin{aligned}\rho_f(\mathbf{r}) = {} & \Lambda_f^{-3}\exp\{c^{(1)}(\mathbf{r},[\rho_s,\rho_f]) \\ & - \beta\int d\mathbf{r}'\rho_f(\mathbf{r})u_{ff}(|\mathbf{r}-\mathbf{r}'|) + \beta\mu \\ & - \beta\int d\mathbf{r}'\rho_s(\mathbf{r})u_{sf}(|\mathbf{r}-\mathbf{r}'|)\}\end{aligned} \tag{13}$$

where $c^{(1)}(\mathbf{r},[\rho_s,\rho_f]) = -\beta\delta F_{ex}[\rho_s(\mathbf{r}),\rho_f(\mathbf{r})]/\delta\rho_f(\mathbf{r})$ depends on both the solid and fluid densities. Here $\beta = 1/k_BT$, k_B is the Boltzmann constant, T is the absolute temperature, $\Lambda_f = h/(2\pi mkT)^{1/2}$ is the thermal de Broigle wavelength, h is the Planck constant, and m is the molecular mass of the fluid molecule.

dx.doi.org/10.1021/la201271p |Langmuir 2011, 27, 6926–6931

Table 2. Lennard-Jones Parameters of Nitrogen and Argon Adsorption on a Silica Surface[32a]

	fluid−fluid parameters		solid−fluid parameters	
adsorbate	ε_{ff}/k_B (K)	$\sigma_{ff} = d_{hs}$ (Å)	ε_{sf}/k_B (K)	σ_{sf} (Å)
N_2 at 77.4 K	95.77	3.549	148.45	3.17
Ar at 87.3 K	111.95	3.358	160.5	3.104

[a] In our calculations, fluid−fluid interactions were truncated at $5\sigma_{ff}$.

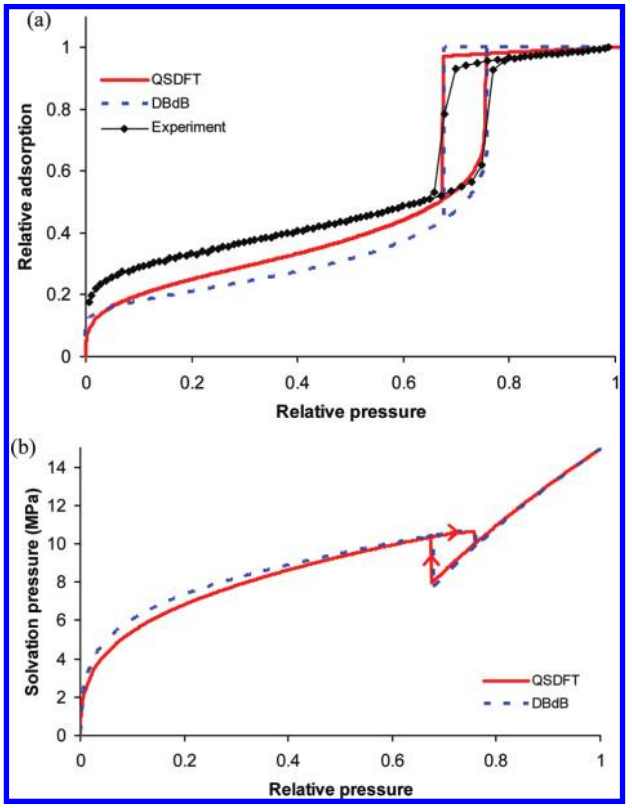

Figure 2. (a) Nitrogen adsorption isotherms. Points: experimental data on SBA-15.[49] Dashed line: DBdB theory predictions for 8.2 nm pore. Solid line: QSDFT theory predictions for 8.2 nm pore. (b) Solvation pressure for nitrogen adsorption. Dashed line: DBdB theory predictions for 8.2 nm pore. Solid line: QSDFT theory predictions for 8.2 nm pore; adsorption and desorption paths are displayed with arrows.

Once the equilibrium distribution of fluid density is determined, its average value gives the adsorption isotherm. The adsorption stress (eq 2) is determined by numerical differentiation of the fluid part of the grand thermodynamic potential (eq 11), in which the fluid equilibrium density is substituted. Since the solid contribution to the grand thermodynamic potential (eq 11) is not subject to variation, it does not contribute to the adsorption stress. This leads to a constant shift of the solvation pressure curve (making $f_s(P = 0) = 0$) and is equivalent to omitting the pre-stress in eq 1. Below in Section 5, the solvation pressure curves obtained using DBdB are shifted in the same fashion for easier comparison. This also allows one to avoid the superfluous parameter γ_{sl}.

5. RESULTS AND DISCUSSION

As a typical example, we studied adsorption of nitrogen at 77.4 K and argon at 87.3 K in cylindrical silica pores of two sizes

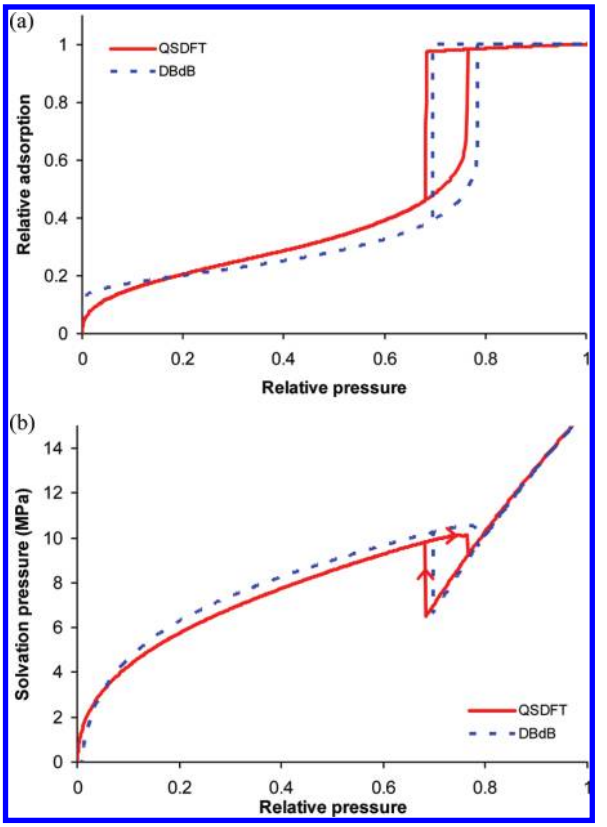

Figure 3. (a) Argon adsorption isotherms for 8.2 nm pore. Dashed line: DBdB theory predictions. Solid line: QSDFT theory predictions. (b) Solvation pressure for argon adsorption. Dashed line: DBdB theory predictions. Solid line: QSDFT theory predictions; adsorption and desorption paths are displayed with arrows.

of 4.0 and 8.2 nm in diameter that are typical for MCM-41 and SBA-15 mesoporous crystals. The adsorption isotherms were calculated using the DBdB and QSDFT methods. The parameters for calculations used in the DBdB method were taken from ref 30 and given in Table 1. For QSDFT calculations, we used the parameters suggested in ref 32: the density profile of the solid is represented as a linear ramp with the half-width $\delta = 4$ Å, the hard sphere diameter of the solid molecule is taken as $d_{hs} = 3$ Å, the number density of the solid is 4.4×10^{28} m^{-3}, and the Lennard-Jones parameters for fluid−fluid and solid−fluid interaction are given in Table 2.

In Figure 2, we present the results for N_2 adsorption in an 8.2 nm pore. Hereinafter, we plot the relative adsorption reduced to the adsorption at saturation pressure, $P/P_0 = 1$. In addition to the theoretical isotherms, the experimental isotherm on the SBA-15 sample[49] is included in Figure 2a to show that both theories quantitatively describe the data in the range of the capillary condensation hysteresis. The noticeable upward shift of the experimental isotherm in the film region can be attributed to the presence of micropores in the SBA-15 sample. The DBdB and QSDFT isotherms perfectly agree, except for an insignificant deviation in the film region.

The DBdB and QSDFT solvation pressure isotherms shown in Figure.2b agree well also. Their nonmonotonic shape reflects the competition between the capillary and Bangham effects. The solvation pressure increases in the film region due to the Bangham effect and then, upon achieving a maximum prior to

dx.doi.org/10.1021/la201271p |Langmuir 2011, 27, 6926–6931

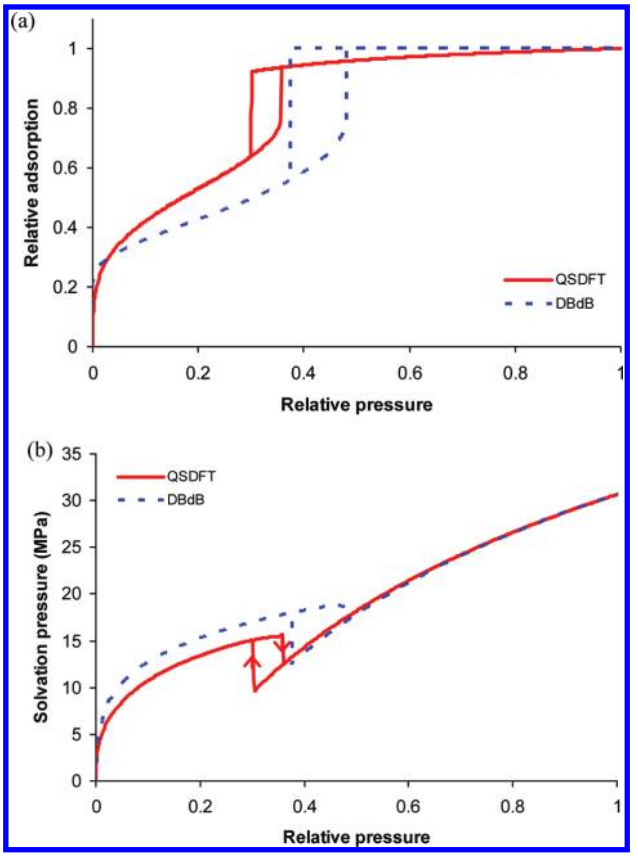

Figure 4. (a) Nitrogen adsorption isotherms for 4.0 nm pore. Dashed line: DBdB theory predictions. Solid line: QSDFT theory predictions. (b) Solvation pressure for nitrogen adsorption. Dash line: DBdB theory predictions. Solid line: QSDFT theory predictions; adsorption and desorption paths are displayed with arrows.

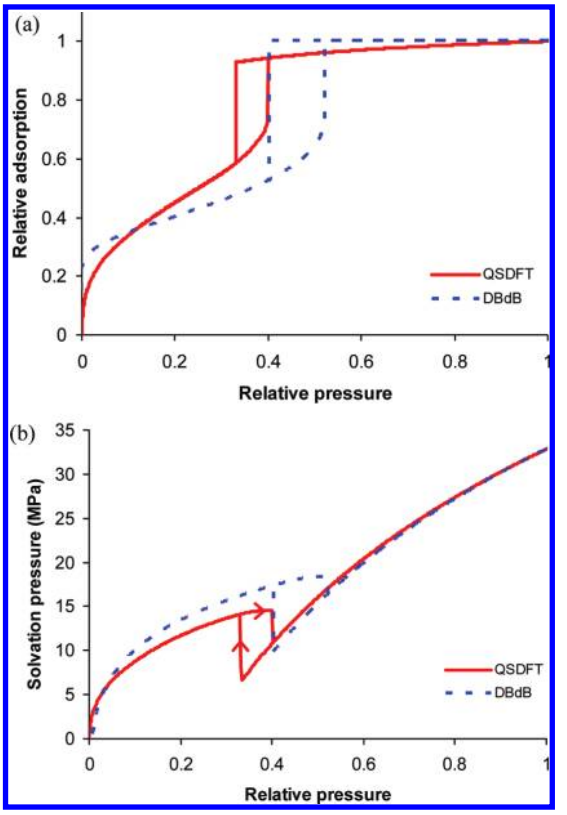

Figure 5. (a) Argon adsorption isotherms for 4.0 nm pore. Dashed line: DBdB theory predictions. Solid line: QSDFT theory predictions. (b) Solvation pressure for argon adsorption. Dashed line: DBdB theory predictions. Solid line: QSDFT theory predictions; adsorption and desorption paths are displayed with arrows.

the capillary condensation, abruptly decreases as the capillary condensation proceeds. In the filled pore region, the solvation pressure increases in accord with the Kelvin−Laplace equation. On the desorption path, the solvation pressure exhibits hysteresis with the minimum achieved at the verge of capillary evaporation. This behavior of the solvation pressure determines the characteristic nonmonotonic variation of the sample volume, which exhibits elastic deformation with expansion as the solvation pressure increases in the course of experiment and contraction as the solvation pressure decreases.

The results of similar calculations for Argon adsorption (Figure 3) confirm that the DBdB theory describes adsorption and solvation pressure isotherms in mesopores of 8.2 nm reasonably well.

Figure 4 and 5 display the calculated adsorption and solvation pressure isotherms in a 4 nm mesopore. The deviations between the DBdB and QSDFT methods are significant because the macroscopic method does not account for the microscopic structure of the adsorbed phase in such tight confinement. The reasons for the inconsistency of the DBdB methods in pores smaller than 7−8 nm were discussed earlier in refs 30 and 31. At the same time, it was shown that the DFT method describes reasonably well the adsorption isotherm in pores as narrow as 4 nm,[32] although the theoretical isotherms exacerbate the hysteresis effect, which in real experiments diminishes in pores smaller than 4 nm (the comprehensive discussion of experimental and theoretically predicted hysteresis loops can be found, e.g., in ref 51). This makes us believe that the QSDFT method can be employed for the analysis of the effects of adsorption deformation in the whole range of mesopores. The experimental data on adsorption deformation of silica mesoporous crystals is scarce, and we cannot confirm this conclusion quantitatively. Indirectly, this conclusion is confirmed by the fact that we were able in our previous work[26] to get a semiquantitative agreement of the DBdB theory for the solvation pressure with the experimental data on water adsorption[24] on the same SBA-15 silica sample[49] with 8.2 nm pores. Unfortunately, we are unable to apply the QSDFT method to process this data, since the water−silica interaction potential is lacking, and we did not want to use it as an adjustable function.

It is worth noting that first attempt to use the QSDFT model for calculating the solvation pressure in the cylindrical mesopore was made in ref 32; however, due to an error in the numeric code, the results presented there were erroneous in the film region.

In conclusions, the QSDFT model is shown to be instrumental for analyses of the variation of the solvation pressure and the respective adsorbent deformation in the course of gas adsorption−desorption cycles on mesoporous materials. The DBdB theory provides an adequate quantitative description for adsorbents with pores larger than ~8 nm and progressively deteriorates in smaller pores. Thus, the QSDFT model can serve as a bridge between the microscopic and macroscopic descriptions.

AUTHOR INFORMATION

Corresponding Author
*E-mail: aneimark@rci.rutgers.edu.

ACKNOWLEDGMENT

G.G. thanks Peter Ravikovitch and Yangzheng Lin for multiple illuminating discussions and help with the QSDFT code. This work was supported in parts by the NSF ERC "Structured Organic Particulate Systems" and the Blaise Pascal International Research Chair fellowship to A.V.N.

REFERENCES

(1) Saussure, H. B. *Essais sur l'Hygrométrie*; Samuel Fauche: Neuchatel, Switzerland, 1783.
(2) Sreznevsky, B. *Jwijev. Sci. Rep. Imp. Univ.* **1895**, 3, as quoted in ref 3.
(3) Whipple, F. J. W. *Proc. Phys. Soc. London* **1921**, *34*, I.
(4) Meehan, F. T. *Proc. R. Soc. London A* **1927**, *115*, 199.
(5) Bangham, D. H.; Fakhoury, N. *Nature* **1928**, *122*, 681.
(6) Haines, R. S.; McIntosh, R. *J. Chem. Phys.* **1947**, *15*, 28.
(7) Amberg, C. H.; McIntosh, R. *Can. J. Chem.* **1952**, *30*, 1012.
(8) Yates, D. J. C. *Proc. R. Soc. London, Ser. A: Math. Phys. Sci.* **1954**, *224*, 526.
(9) Scherer, G. W. *J. Am. Ceram. Soc.* **1986**, *69*, 473.
(10) Bering, B. P.; Krasilnikova, O. K.; Sarakhov, A. I.; Serpinskii, V. V.; Dubinin, M. M. *Bull. Acad. Sci. USSR Div. Chem. Sci.* **1977**, *26*, 2258.
(11) Krasilnikova, O. K.; Bering, B. P.; Serpinskii, V. V.; Dubinin, M. M. *Bull. Acad. Sci. USSR Div. Chem. Sci.* **1977**, *26*, 1099.
(12) Bering, B. P.; Krasilnikova, O. K.; Serpinskii, V. V. *Bull. Acad. Sci. USSR Div. Chem. Sci.* **1978**, *27*, 2515.
(13) Smith, D. M.; Scherer, G. W.; Anderson, J. M. *J. Non-Cryst. Solids* **1995**, *188*, 191.
(14) Dolino, G.; Bellet, D.; Faivre, C. *Phys. Rev. B* **1996**, *54*, 17919.
(15) Lawnik, W. H.; Goepel, U. D.; Klauk, A. K.; Findenegg, G. H. *Langmuir* **1995**, *11*, 3075.
(16) Muroyama, N.; Yoshimura, A.; Kubota, Y.; Miyasaka, K.; Ohsuna, T.; Ryoo, R.; Ravikovitch, P. I.; Neimark, A. V.; Takata, M.; Terasaki, O. *J. Phys. Chem. C* **2008**, *112*, 10803.
(17) Boutin, A.; Springuel-Huet, M.-A.; Nossov, A.; Gédéon, A.; Loiseau, T.; Volkringer, C.; Férey, G.; Coudert, F.-X.; Fuchs, A. H. *Angew. Chem., Int. Ed.* **2009**, *48*, 8314.
(18) Neimark, A. V.; Coudert, F. X.; Boutin, A.; Fuchs, A. H. *J. Phys. Chem. Lett.* **2010**, *1*, 445.
(19) Bangham, D. H.; Fakhoury, N. *Proc. R. Soc. London, Ser. A* **1930**, *130*, 81.
(20) Bangham, D. H. *Trans. Faraday Soc.* **1937**, *33*, 805.
(21) Mogilnikov, K. P.; Baklanov, M. R. *Electrochem. Solid State Lett.* **2002**, *5*, F29.
(22) Dourdain, S.; Britton, D. T.; Reichert, H.; Gibaud, A. *Appl. Phys. Lett.* **2008**, *93*, 183108.
(23) Guenther, G.; Prass, J.; Paris, O.; Schoen, M. *Phys. Rev. Lett.* **2008**, *101*, 086104.
(24) Prass, J.; Muter, D.; Fratzl, P.; Paris, O. *Appl. Phys. Lett.* **2009**, *95*, 083121.
(25) Balzer, C.; Wildhage, T.; Braxmeier, S.; Reichenauer, G.; Olivier, J. P. *Langmuir* **2011**, *27*, 2553.
(26) Gor, G. Y.; Neimark, A. V. *Langmuir* **2010**, *26*, 13021.
(27) Derjaguin, B. V. *Acta Physicochim. URSS* **1940**, *12*, 181.
(28) Broekhoff, J. C. P.; de Boer, J. H. *J. Catal.* **1967**, *9*, 8.
(29) Broekhoff, J. C. P.; De Boer, J. H. *J. Catal.* **1967**, *9*, 15.
(30) Neimark, A. V.; Ravikovitch, P. I. *Microporous Mesoporous Mater.* **2001**, *44*, 697.
(31) Neimark, A. V.; Ravikovitch, P. I.; Vishnyakov, A. *J. Phys.: Condens. Matter* **2003**, *15*, 347.
(32) Ravikovitch, P. I.; Neimark, A. V. *Langmuir* **2006**, *22*, 11171.
(33) Neimark, A. V.; Lin, Y. Z.; Ravikovitch, P. I.; Thommes, M. *Carbon* **2009**, *47*, 1617.
(34) Rusanov, A. I.; Kuni, F. M. *Russian J. Gen. Chem.* **2007**, *77*, 371.
(35) Mushrif, S. H.; Rey, A. D. *Chem. Eng. Sci.* **2009**, *64*, 4744.
(36) Vandamme, M.; Brochard, L.; Lecampion, B.; Coussy, O. *J. Mech. Phys. Solids* **2010**, *58*, 1489.
(37) Ravikovitch, P. I.; Neimark, A. V. *Langmuir* **2006**, *22*, 10864.
(38) Kowalczyk, P.; Ciach, A.; Neimark, A. V. *Langmuir* **2008**, *24*, 6603.
(39) Yang, K.; Lu, X. C.; Lin, Y. Z.; Neimark, A. V. *Energy Fuels* **2010**, *24*, 5955.
(40) Balbuena, P. B.; Berry, D.; Gubbins, K. E. *J. Phys. Chem.* **1993**, *97*, 937.
(41) Herman, T.; Day, J.; Beamish, J. *Phys. Rev. B* **2006**, *73*, 094127.
(42) Frenkel, J. I. *Kinetic Theory of Liquids*; Oxford University Press: London, 1946.
(43) Halsey, G. *J. Chem. Phys.* **1948**, *16*, 931.
(44) Hill, T. L.; Frankenburg, W. G.; Komarewsky, V. I.; Rideal, E. K. *Theory of Physical Adsorption*; Academic Press: New York, 1952; Vol. 4, p 211.
(45) Lastoskie, C.; Gubbins, K. E.; Quirke, N. *J. Phys. Chem.* **1993**, *97*, 4786.
(46) Ravikovitch, P. I.; O'Domhnaill, S. C.; Neimark, A. V.; Schuth, F.; Unger, K. K. *Langmuir* **1995**, *11*, 4765.
(47) Rosenfeld, Y. *Phys. Rev. Lett.* **1989**, *63*, 980.
(48) Rosenfeld, Y.; Schmidt, M.; Lowen, H.; Tarazona, P. *Phys. Rev. E* **1997**, *55*, 4245.
(49) Jahnert, S.; Muter, D.; Prass, J.; Zickler, G. A.; Paris, O.; Findenegg, G. H. *J. Phys. Chem. C* **2009**, *113*, 15201.
(50) Neimark, A. V.; Ravikovitch, P. I.; Vishnyakov, A. *Phys. Rev. E* **2000**, *62*, R1493.
(51) Neimark, A. V.; Ravikovitch, P. I.; Vishnyakov, A. *Phys. Rev. E* **2002**, *65*, 031505.